

NASA TECHNICAL
MEMORANDUM

NASA TM X-62,087

NASA TM X-62,087

TIP VORTICES - VELOCITY DISTRIBUTIONS

N. A. Chigier and V. R. Corsiglia

Ames Research Center
Moffett Field, Calif. 94035

September 1971

FACILITY FORM 602

N71-36679
(ACCESSION NUMBER)
14
(PAGES)
TMX 62087
(NASA CR OR TMX OR AD NUMBER)

(THRU)
G3

(CODE)
12

(CATEGORY)



TIP VORTICES - VELOCITY DISTRIBUTIONS

N. A. Chigier* and V. R. Corsiglia**
Ames Research Center, NASA
Moffett Field, California 94035

Abstract

Detailed measurements of velocity distributions have been made in vortices generated at the tip of a square-tip, 18-inch-chord, 48-inch semispan blade mounted in the NASA-Ames 7-by-10-Foot Wind Tunnel. Time-mean-average velocity components were measured using a triple-sensor hot wire probe operated by three separate anemometers. With the blade at an angle of attack of 12° , traverses were made through the vortex centers at six axial stations, $x/c = -0.75, -0.50, -0.25, 0.0, 2.0,$ and 4.0 , where $x/c = 0$ is the trailing edge.

The dimensions of the vortex increase with distance downstream over the blade surface, and at $x/c = 4$ the vortex core radius is 1.7% of the span. Maximum circumferential velocity is 42% of mainstream velocity was measured at $x/c = -0.50$, over the wing surface, followed by decay to 24.0% of mainstream velocity at $x/c = 4$. Axial velocity in excess of free-stream velocity was measured in the vortex core with maximum axial velocity of 140% of free-stream velocity at $x/c = -0.25$. The vortex center moved inward from the tip at $x/c = -0.75$ to 2.9% of span at $x/c = 4$. A secondary vortex was located outboard of the main tip vortex.

Notation

a	core radius - radius where u_θ is a maximum
A	aspect ratio
b	wing span
c	chord
c_l	local lift coefficient
c_p	local pressure coefficient
C_L	lift coefficient
C_D	drag coefficient
e	distance to roll up (from trailing edge)
M	Mach number
r	radial coordinate from vortex center
Re_c	Reynolds number based on chord

Presented at the 27th Annual National Forum of the American Helicopter Society, May 1971.

*National Research Council Senior Associate. On leave of absence from Department of Chemical Engineering, University of Sheffield, England.

**Research Scientist.

u	time-mean-average velocity
V_∞	mainstream velocity
x	streamwise ordinate, aft from trailing edge
y	spanwise ordinate, inboard from wing tip
z	normal ordinate, above upper wing surface from trailing edge
α	angle of attack, deg
Γ	circulation at radius r
Γ_0	circulation around the wing
ω	angular velocity
ζ	local vorticity

Subscripts

o	initial value or median section
r	radial with respect to vortex center
x	axial, streamwise
y	spanwise
z	normal
θ	circumferential
max	maximum value

Introduction

Operating characteristics of rotating wing devices, such as helicopter rotors, aircraft propellers, and V/STOL propeller rotors, are strongly influenced by vortex wakes. The interaction of an individual blade with a vortex wake changes the aerodynamic load on the blade and thus affects the blade's operating performance, vibration, and noise characteristics. One of the major sources of noise generation in helicopters is a rotor blade passing near or through a vortex trailed at the tip of another blade.¹ At low forward speeds a sharp cracking sound called blade slap results from very rapid time rates of change in local blade pressure distribution due to angle-of-attack change which occurs when a blade passes through or very close to a trailing tip vortex from a preceding blade. Blade slap, when it occurs, becomes the predominant external noise associated with the aircraft and plays a major role in determining aircraft detectability and in setting the low-frequency end of the noise spectrum.¹ The magnitude of blade slap depends on the

maximum induced velocities encountered by the blades, the size of the vortex core, and the proximity of the blade to the vortex core.

Previous experimental studies of blade tip vortices have used smoke^{2,3} for visualization of vortices and oil or acenaphthene⁴ for visualization of blade surface flow. Location of the vortices is inferred from these visualization experiments, and it is generally presumed that the smoke tracer is concentrated in the vortex core. Spivey⁵ concluded from a comparison of tip vortices on rotating and on nonrotating blades that the location and direction of vortices are not affected by centrifugal force or pressure gradients. We can therefore expect that the vortex structure determined in the wind tunnel tests reported in this paper will be the same on a rotating blade in hover at low Mach number.

This paper reports on detailed measurements, made with hot wire anemometers, of magnitudes of streamwise, spanwise, and normal velocity components of a wing tip vortex. The measurements made on a fixed wing in a wind tunnel, covered the region of vortex generation over the wing surface and the rollup region to four chord lengths downstream of the trailing edge. Until vortex velocity distributions are measured on rotating blades, we may predict flow fields under flight conditions by superposing the vortex flow field as determined from the present experiments on the flow fields generated by forward flight of the aircraft and rotation of the blade.

Apparatus

Figure 1 is a schematic diagram of the experimental apparatus. A rectangular wing of NACA 0015 airfoil section with a thickened trailing edge was mounted vertically in the Ames 7- by 10-Foot Wind Tunnel. The end surface of the wing tip was flat. Wing characteristics and test conditions were as follows:

c	= 18 in.
$b/2$	= 48 in.
A	= 5.33
V_{∞}	= 100 ft/sec
Re_c	= 9.53×10^5
M	= 0.09
α	= 12°
C_L	= 0.72

The wing was the same as that used by Spivey and Morehouse.⁴

A triple-sensor hot-wire probe consisting of three wires placed in a three-axis array with 90° between them (Fig. 2) was operated by three separate constant-temperature anemometers. Measurements were effectively averaged over a region 2 mm in diameter. Traverses were made parallel and normal to the spanwise direction, through the vortex centers, using a remote controlled traversing mechanism, with the probe retained at successive points for times sufficient to take time mean averages. Traverses were made at six axial stations, $x/c = -0.75, -0.50, -0.25, 0.00, 2.00, \text{ and } 4.00$, where $x/c = 0$ is the trailing edge. Each wire of the probe was calibrated as a function of wind-tunnel speed before and after each traverse. Measured mean voltages were corrected for air temperature variation, and magnitudes of streamwise, spanwise, and normal

velocity components were calculated from measured time average velocities.

Measurements

Surface Pressure

The surface pressure measurements made by Spivey,⁴ (Fig. 3) show that in the tip region, $y/b < 0.04$, low pressure peaks begin at $x/c = -0.75$ at the tip and move inboard and aft (Fig. 3(b)). This suction on the upper surface at the tip, associated with the vortex, is sufficiently large to raise the load at the tip to that on the remainder of the wing and transform the span loading from an approximate elliptic distribution to a distribution approaching rectangular (Fig. 3(c)). This tip-vortex augmented lift and its effect on the span loading will help to explain differences between measured vortex core size and location, and those predicted by Spreiter and Sacks.⁶ The additional suction peaks at $y/b = 0.007$ and 0.004 (Fig. 3) near the trailing edge are due to a secondary vortex detected by chemical film surface visualization and by the hot wire measurements (discussed later).

Velocity Distributions

The approximate symmetry of measurements about the vortex center at $x/c = 4.0$ and 2.0 allowed the adoption of a cylindrical coordinate system and resolution of velocity into axial, circumferential, and radial components. At the trailing edge and over the wing surface this symmetry is distorted by the accelerating streamwise flow and the inboard spanwise flow over the top surface of the wing. Further, over the wing surface the inclination of the vortex to the wind tunnel axis is of the order of 10° . Calculation of u_θ , u_r , and u_x with respect to the vortex coordinate system requires correction which takes into account transformation of the coordinates. This has not been done in the data presented. Figure 4 shows the circumferential velocity u_θ normalized with the mainstream velocity V_{∞} as a function of normal distance z/b . The experimental data are sufficiently detailed for the vortex to be clearly detected as a solid-body-rotation core with $u_\theta = \omega r$ surrounded by a 'potential' vortex with u_θ inversely proportional to r . Over the wing surface the vortex was measured by approaching to within $3/32$ in. from the upper surface. The location of the vortex center is defined by the position where $u_\theta = 0$ and the core radius, a , is defined as the distance from the vortex center to the radius where u_θ is a maximum. The vortex center through which surveys were made can be found for each traverse by reference to Figures 14 and 15.

Spanwise distributions u_θ are shown in Figure 5. The vortex at $x/c = -0.75$ can be clearly detected so that the point origin of the vortex can be assumed to be a short distance upstream of $x/c = -0.75$. The presence of a secondary vortex can be detected from the distributions of u_θ in Figure 5 at $x/c = -0.25$ and $x/c = 0$. The secondary vortex is smaller and weaker than the main vortex, rotating in the same direction as the main vortex and located between the main vortex and the tip. The location of the secondary vortex is the same as that found by Spivey and Morehouse⁴ from surface chemical film visualization.

Axial Velocities

Visualization of vortices by helium balloons⁷ and in water-towing tanks⁸ have indicated the presence of axial velocities toward the wing of the order of 11% of wing speed. The presence of axial velocity in the vortex requires the vortex to be considered as three dimensional. Axial velocities will affect the persistence and dissipation⁹ of the vortex, stability,¹⁰ and turbulence generation, in a manner which is not yet clearly understood. Attempts to increase axial flow by blowing or to reduce axial flows by introducing bluff body dissipators¹¹ have been shown to promote disintegration or dissipation of the vortices.

Measured axial (streamwise) velocities u_x/V_∞ are shown in Figure 6 as a function of normal position z/b . Maximum axial velocities occur, in all cases measured, at the vortex center and are in excess of the mainstream velocity V_∞ (i.e., under flight conditions, in a direction away from the wing). The axial velocities over the wing upper surface are directly associated with the acceleration of flow caused by the streamwise pressure gradients. In the 'two-dimensional' region of the wing, away from the tip, magnitudes of measured axial velocities agree with those calculated from surface pressure using the Bernoulli equation. In the tip region pressure gradients exist through the vortex to balance the centrifugal forces, and streamlines curve in more than one direction. Therefore, there is no simple correlation between surface pressure measurements and the flow field. Axial accelerations occur in the vortex core in addition to accelerations that would be expected from linear wing theory. The axial velocity distributions in Figure 6 show velocity defects ($u_x/V_\infty < 1.0$) outside the vortex core at the trailing edge ($x/c = 0$) and downstream ($x/c > 0$). The largest magnitudes of the axial velocity defect were measured in the spanwise traverse along the trailing edge. The axial velocity defect is, therefore, associated with the wake and drag of the wing. Turbulence is generated under the shearing action of the axial velocity gradients, and maximum turbulence intensities were measured at the points of maximum circumferential velocity which coincide with the regions of maximum axial velocity gradient. Under the influence of the turbulence in the core, momentum will be exchanged radially so that we could expect downstream decay of the excess axial velocity.

Spanwise distributions of u_x (Fig. 7) show more clearly the influence of acceleration over the wing upper surface and velocity defect associated with separation and the wake. At $x/c = -0.75$ the streamwise acceleration can be seen over the wing surfaces where the maximum value of $u_x/V_\infty = 1.32$ has the same magnitude as the velocity calculated from the pressure measurements, $u_x/V_\infty = (1 - c_p)^{1/2}$. Velocity defect, indicating separation, was measured at $x/c = -0.25$ while at the trailing edge ($x/c = 0$), velocity defects, indicating the turbulent wake, were measured at all spanwise positions outside the vortex core.

Normal and Spanwise Velocity

Distributions of u_z (Fig. 8) show curvature of streamlines following the contour of the wing upper surface at $x/c = -0.75$ and -0.5 . At $x/c = -0.25$ and 0 streamlines curve away from the wing surface ($u_z/V_\infty > 0$), indicating separation of the flow. At $x/c = 2$ and 4 , values of u_z have declined to virtually zero.

Crossflow (sidewash) is shown by the spanwise distributions of u_y in Figure 9. Over the wing surface, flow is predominantly inboard from the tip with a maximum value of $u_y/V_\infty = 0.33$ at $x/c = -0.5$. The negative values of u_y (Fig. 9) are associated with the interaction of the main vortex with the wake and the secondary vortex. Relative orders of magnitude of velocity components are shown for $x/c = 3.75$ in Figure 10.

Vortex Rollup

Spreiter and Sacks⁶ made theoretical predictions of vortex rollup and found that the degree to which vortices are rolled up depends upon the distance behind the wing, the lift coefficient, span loading, and aspect ratio of the wing according to the equation

$$e/c = K(A/C_L)(b/c)$$

The constant K has the value $K = 0.28$ for wings having elliptic span loading which results in a distance to rollup $e/c = 11.0$ for the wing used in these experiments. However, if the span loading is other than elliptical the vortices will roll up faster if more load is concentrated near the wing tips. For rectangular wings the Spreiter and Sacks⁶ calculations yield a value of $e/c = 3.6$. On the basis of the assumptions and calculations of Spreiter and Sacks,⁶ then, we may expect rollup to have occurred before the axial station of $x/c = 4$. Figure 10 shows the normal distribution of axial, circumferential and radial components of velocity at $x/c = 3.75$. Plotting values of u_θ constant, from the normal and spanwise traverse, in the yz -plane at $x/c = 4$ shows the flow to be reasonably symmetric about the vortex center. Further, values of the radial component (u_y for spanwise traverse and u_z for normal traverse) are essentially zero. Therefore, the local circulation may be taken to be

$$\Gamma = 2\pi r u_\theta$$

and the local vorticity

$$\zeta = (1/r)(d/dr)(ru_\theta) = (du_\theta/dr) + (u_\theta/r)$$

Circulation around the wing is determined from the local lift coefficient at the median section obtained by integration of surface pressure measurements according to the equation:

$$\Gamma_0 = (1/2)V_\infty c_l c_{l_0}$$

This gives a value of $\Gamma_0 = 49.8 \text{ ft}^2/\text{sec}$.

Estimates of circulation obtained by assuming axial symmetry at $x/c = 2$ and 4 give values of Γ_{max} approximately equal to $30 \text{ ft}^2/\text{sec}$.

Table 1 shows the distance to rollup, the inboard displacement of vortex core y_c/b , and core radius a_c/b , predicted by Spreiter and Sacks for elliptic and actual loading compared with those obtained in the present experiment.

Table 1

	e/c	y_c/b	a/b
Spreiter and Sacks			
Elliptic loading	11.0	0.107	0.078
Actual loading	3.6		0.012
Present experiment	4.0	0.029	0.017

As noted in Table 1 the predictions of Spreiter and Sacks are very sensitive to span loading so that if measured values of C_D , C_L , and y_c/b are used the predicted value of a/b will agree closely with our measurements.

Downstream Development of Vortex

The downstream development of the vortex is presented in Figures 11-15 in which significant vortex parameters are plotted as functions of x/c . A maximum circumferential velocity of 42.2% of mainstream velocity was measured at the midchord station (Fig. 11), followed by a decay to 24% at $x/c = 4$. The maximum value of axial velocity (139% of mainstream velocity) was measured at $x/c = -0.25$ (Fig. 12), followed by a rapid deceleration in the trailing-edge region. Core radius determined from radial distance to $u_{\theta \max}$ increases over the wing surface (Fig. 13) and reaches a maximum of $a/b = 1.33\%$ at $x/c = 4$. The vortex centerline moves inboard from the tip at $x/c = -0.75$ (Fig. 14) to a value of $y_c/b = 2.9\%$ at $x/c = 4$. As the vortex grows in size the vortex centerline lifts off the wing upper surface (Fig. 15) and at $x/c = 4$, $z_c/b = 1.46\%$.

Conclusions

Maximum circumferential velocities of 42% of mainstream velocity are generated in the tip vortex at the midchord of a rectangular wing, and decay to 24% of mainstream velocity at rollup. Axial velocity in excess of free-stream velocity (equivalent to axial flow downstream away from the wing under flight conditions) exists in the vortex core from generation of the vortex, at 1/4 chord from the leading edge, to four chord lengths downstream of the wing trailing edge ($x/c = 4$). Maximum axial velocity of 140% of mainstream velocity was measured over the wing upper surface ($x/c = -0.25$), and decayed to 120% at $x/c = 4$. These axial velocity excesses are associated with the streamwise acceleration over the wing upper surface.

At ($x/c = 4$) the vortex core radius, 1.3% of span, is an order of magnitude smaller than that predicted by Spreiter and Sacks assuming elliptic span loading. However, if the actual span loading is used then the Spreiter and Sacks prediction agrees quite closely with the measurement. Separation of the vortex centers at rollup is 94.2% of span compared to the classical prediction of $\pi/4$ or 78.5% for elliptic loading. Tip vortices generate lift in the tip region, so that the span loading on a rectangular wing differs significantly from that predicted by linear theory. When account is taken of the augmentation in lift at the tip, the measured increase in vortex separation and reduced size of core can be explained.

A secondary vortex of lesser strength and smaller core than the main tip vortex is generated over the wing upper surface between the main vortex and the tip. The secondary

vortex rotates in the same direction as the main vortex and is absorbed by the main vortex during rollup.

Acknowledgements

This work was undertaken while one of the authors held a National Research Council Senior Postdoctoral Resident Research Association supported by the National Aeronautics and Space Administration at NASA-Ames Research Center, Moffett Field, California. The authors wish to thank Mark Kelly, Chief of the Large Scale Aerodynamics Branch at Ames for many helpful suggestions and discussions; Miss J. Frick and Miss B. Barclay for valuable assistance in computation and G. G. Morehouse for permission to use the rotor blade and pressure measurements.

References

1. USAAVLABS Technical Report 66-1, TIP VORTEX CORE THICKENING FOR APPLICATION TO HELICOPTER ROTOR NOISE GENERATION, Spencer, R. H., Sternfield, H., McCormick, B. W., U.S. Army Aviation Material Laboratories, Ft. Eustis, Virginia, September 1966.
2. Cornell Aeronautical Laboratory Report AC-2647-S-1, AN EXPERIMENTAL STUDY OF BLADE TIP VORTICES, Piziali, R., and Trenka, A., Cornell Aeronautical Laboratory, Buffalo, New York, January 1970.
3. Spencer, R. H., APPLICATION OF VORTEX VISUALIZATION TEST TECHNIQUES TO ROTOR NOISE RESEARCH, 26th Annual National Forum of the American Helicopter Society, Washington, D. C., June 1970.
4. Spivey, W. A. and Morehouse, G. G., NEW INSIGHTS INTO THE DESIGN OF SWEEP-TIP ROTOR BLADES, 26th Annual National Forum of the American Helicopter Society, Washington, D. C., June 1970.
5. Spivey, R. F., BLADE TIP AERODYNAMICS - PROFILE AND PLANFORM EFFECTS, 24th Annual National Forum, American Helicopter Society, Washington, D. C., May 1968.
6. Spreiter, J. R., and Sacks, A. H., THE ROLLING UP OF THE TRAILING VORTEX SHEET AND ITS EFFECT ON THE DOWNWASH BEHIND WINGS, Journal of the Aeronautical Sciences, January 1951, pp. 21-32.
7. MacCready, P. B., AN ASSESSMENT OF DOMINANT MECHANISMS IN VORTEX-WAKE DECAY, Symposium on Aircraft Wake Turbulence, Seattle, Washington, September 1970.
8. Olson, J. H., RESULTS OF TRAILING VORTEX STUDIES IN A TOWING TANK, Boeing Scientific Research Laboratories D1-82-1004, September 1970.
9. Batchelor, G. K., AXIAL FLOW IN TRAILING LINE VORTICES, Journal of Fluid Mechanics, Vol. 20, 1964, p. 20.

10. Parks, P. C., A NEW LOOK AT THE DYNAMICS OF VORTICES WITH FINITE CORES, Symposium on Aircraft Wake Turbulence, Seattle, Washington, September 1970.

11. Corsiglia, V. R., Jacobsen, R. A., and Chigier, N. A., AN EXPERIMENTAL INVESTIGATION OF TRAILING VORTICES BEHIND A WING WITH A VORTEX DISSIPATOR, Symposium on Aircraft Wake Turbulence, Seattle, Washington, September 1970.

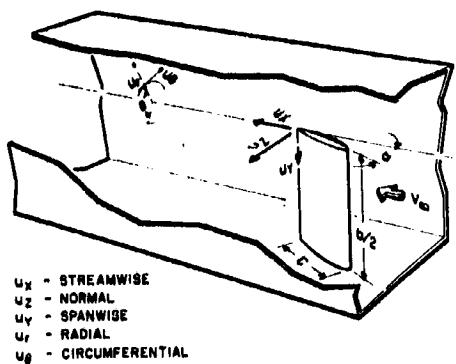


Figure 1.- Rectangular square-tip wing mounted vertically in NASA - Ames 7-by-10-Foot Wind Tunnel.

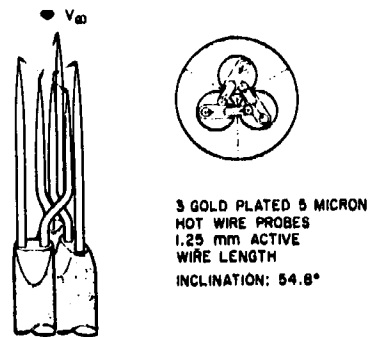
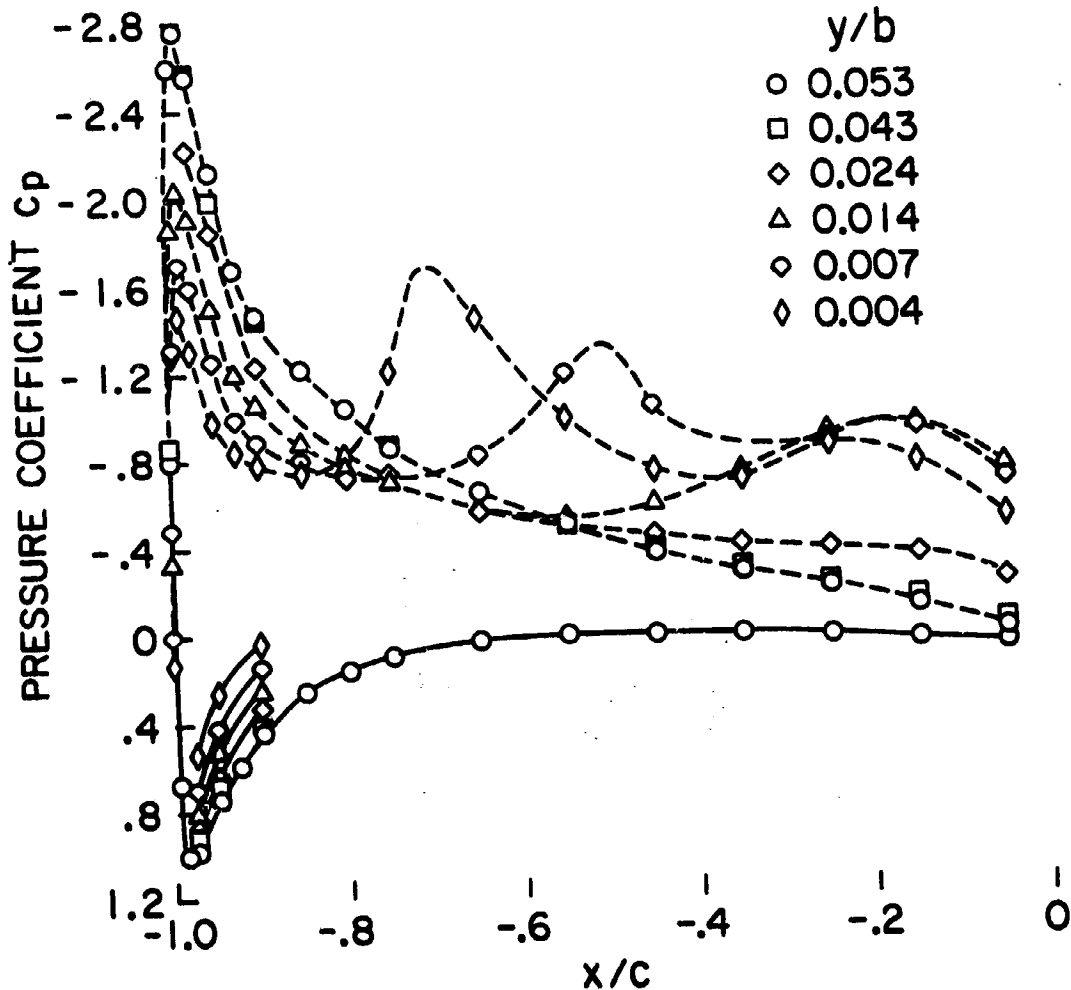
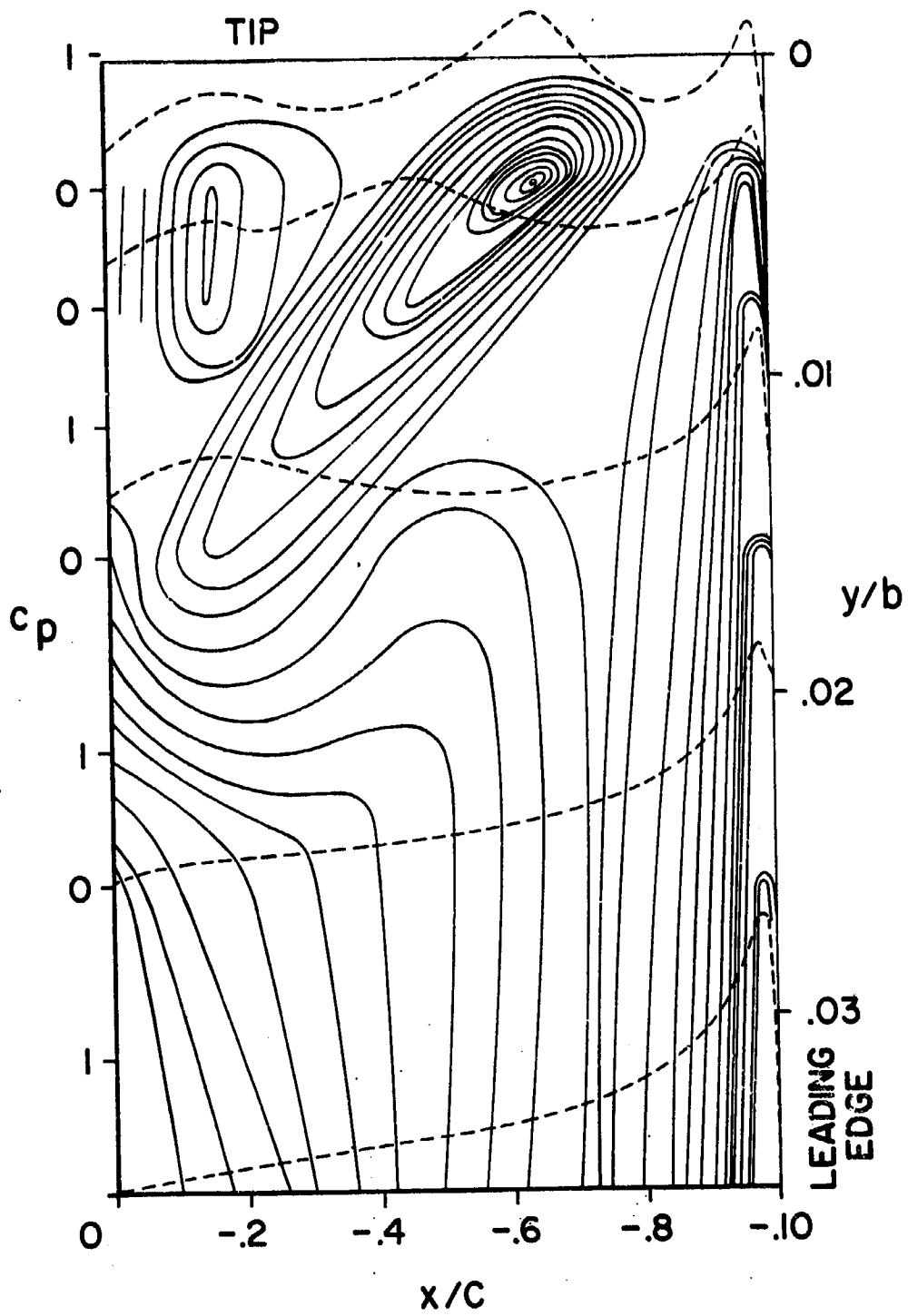


Figure 2.- Hot wire probe for three-dimensional flow measurement.



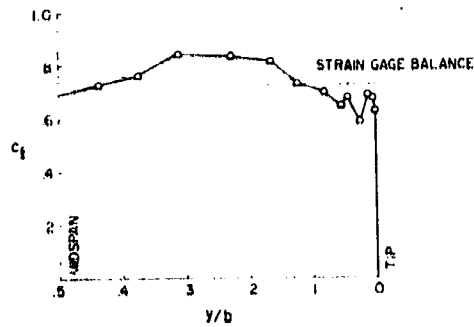
(a) Distribution of pressure coefficient over upper and lower surfaces of wing in tip region.

Figure 3.- Pressure distribution on wing surface.



(b) Isobars on top surface of wing (tip region).

Figure 3.- Continued.



(c) Span loading based on integration of measured surface pressure distributions.

Figure 3.— Concluded.

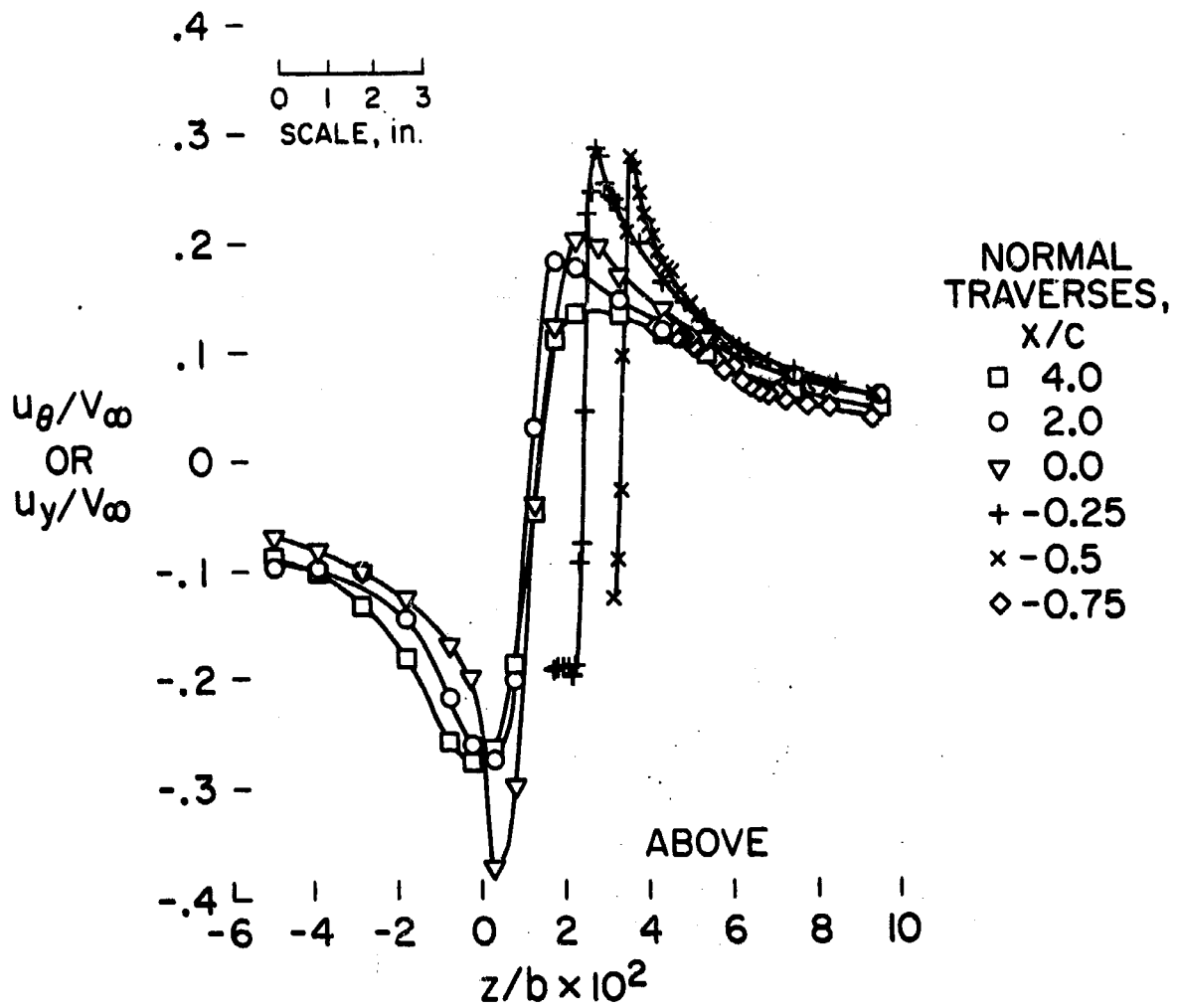


Figure 4.— Normal distribution of circumferential velocity.

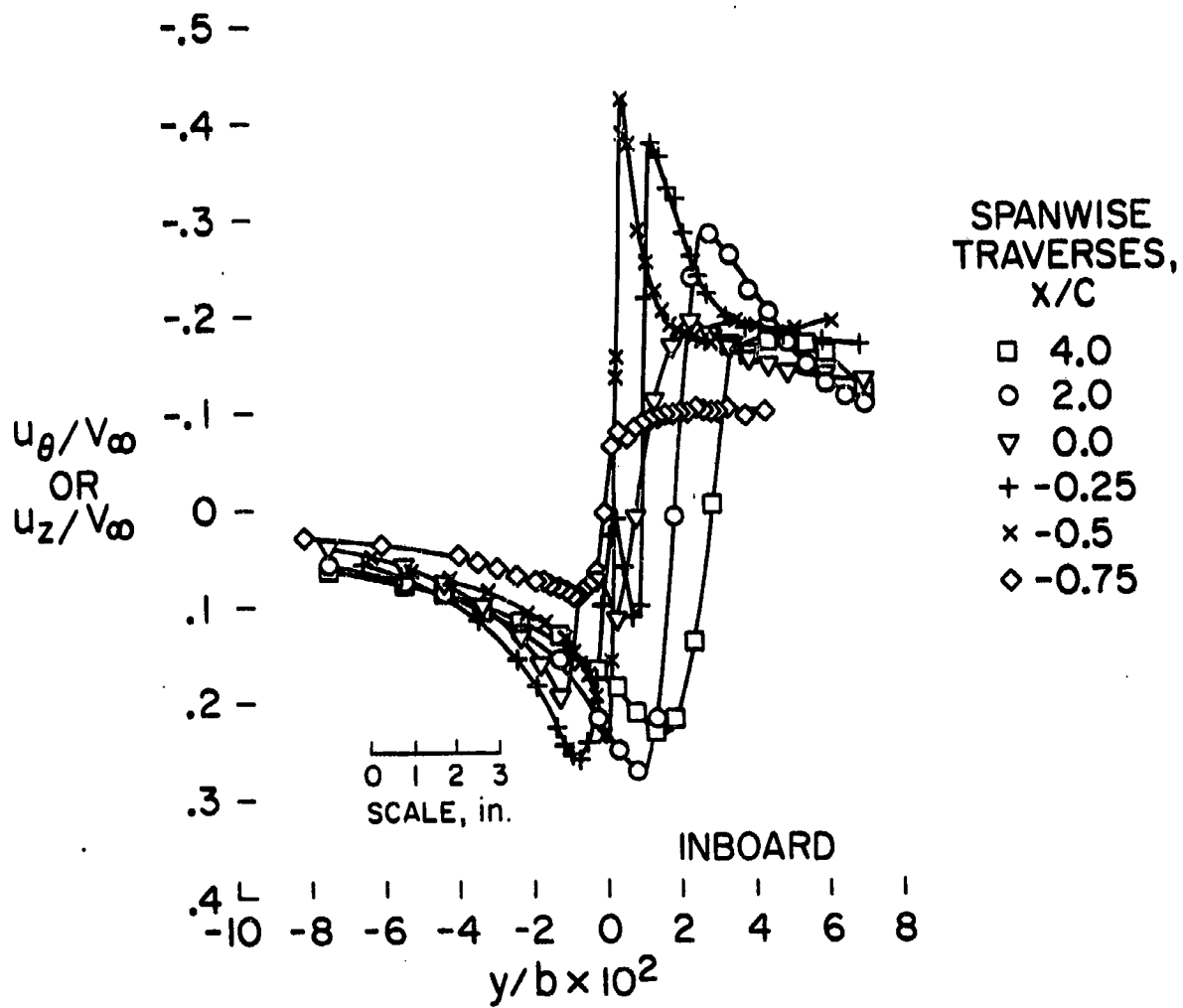


Figure 5.— Spanwise distribution of circumferential velocity.

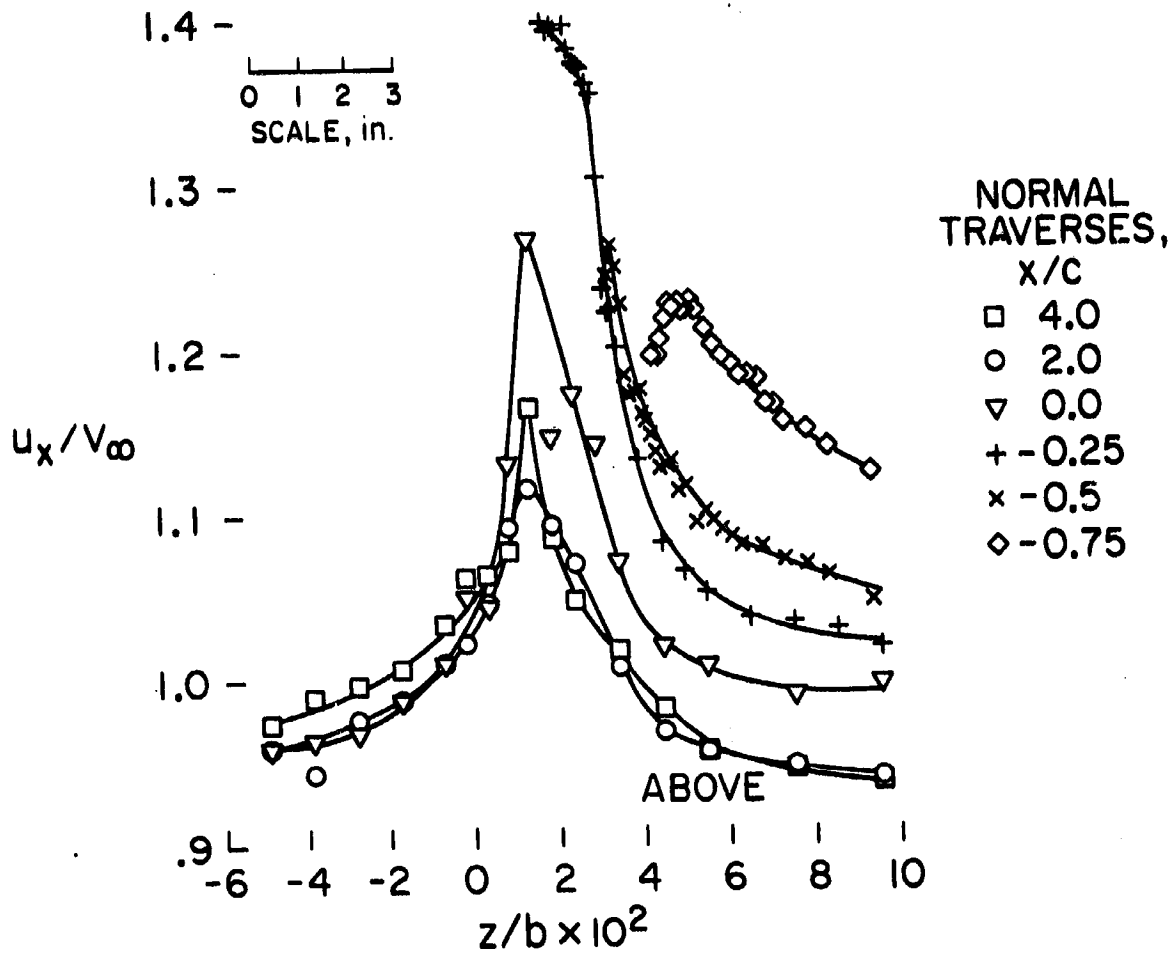


Figure 6.— Normal distribution of streamwise velocity.

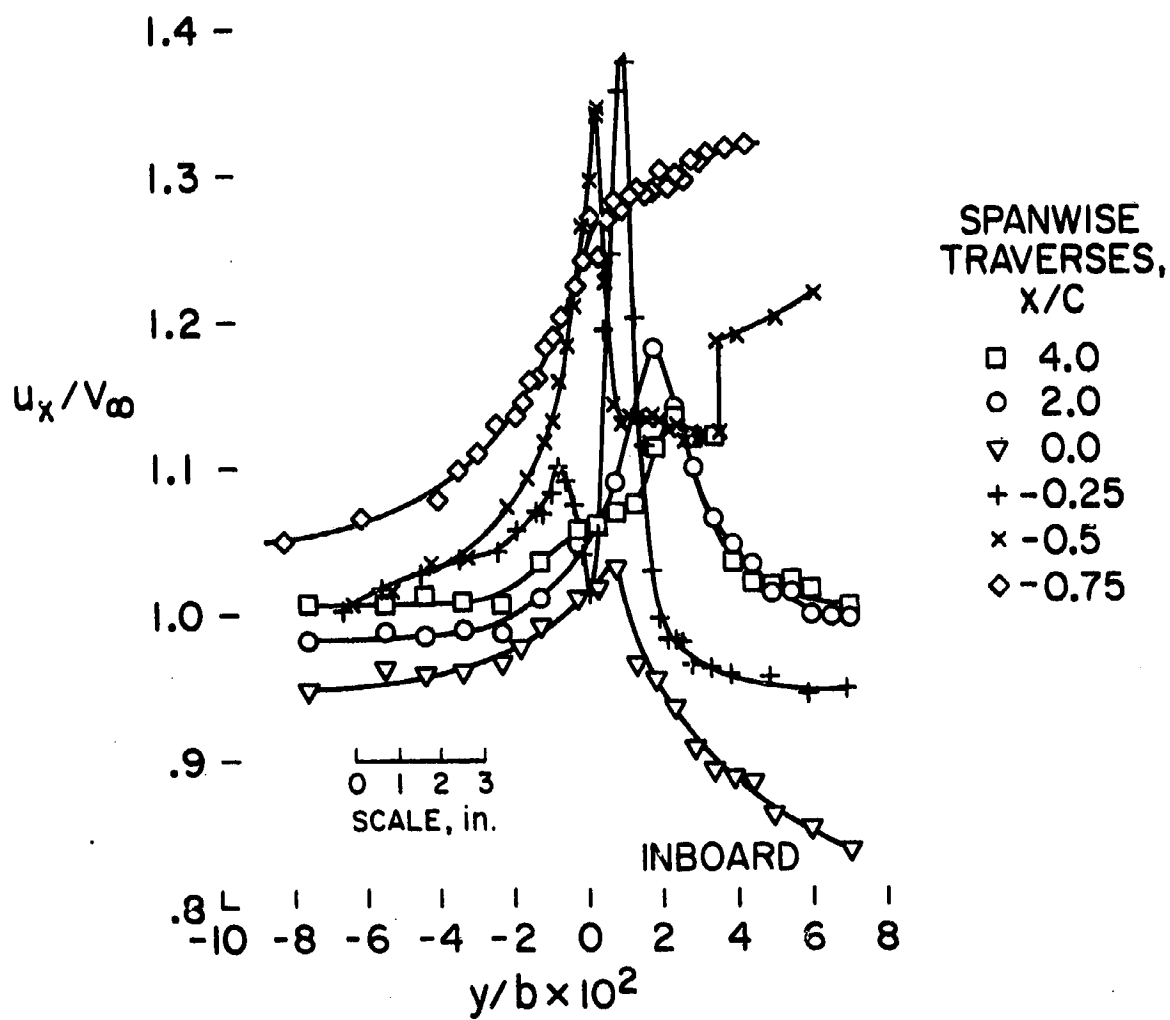


Figure 7.— Spanwise distribution of streamwise velocity.

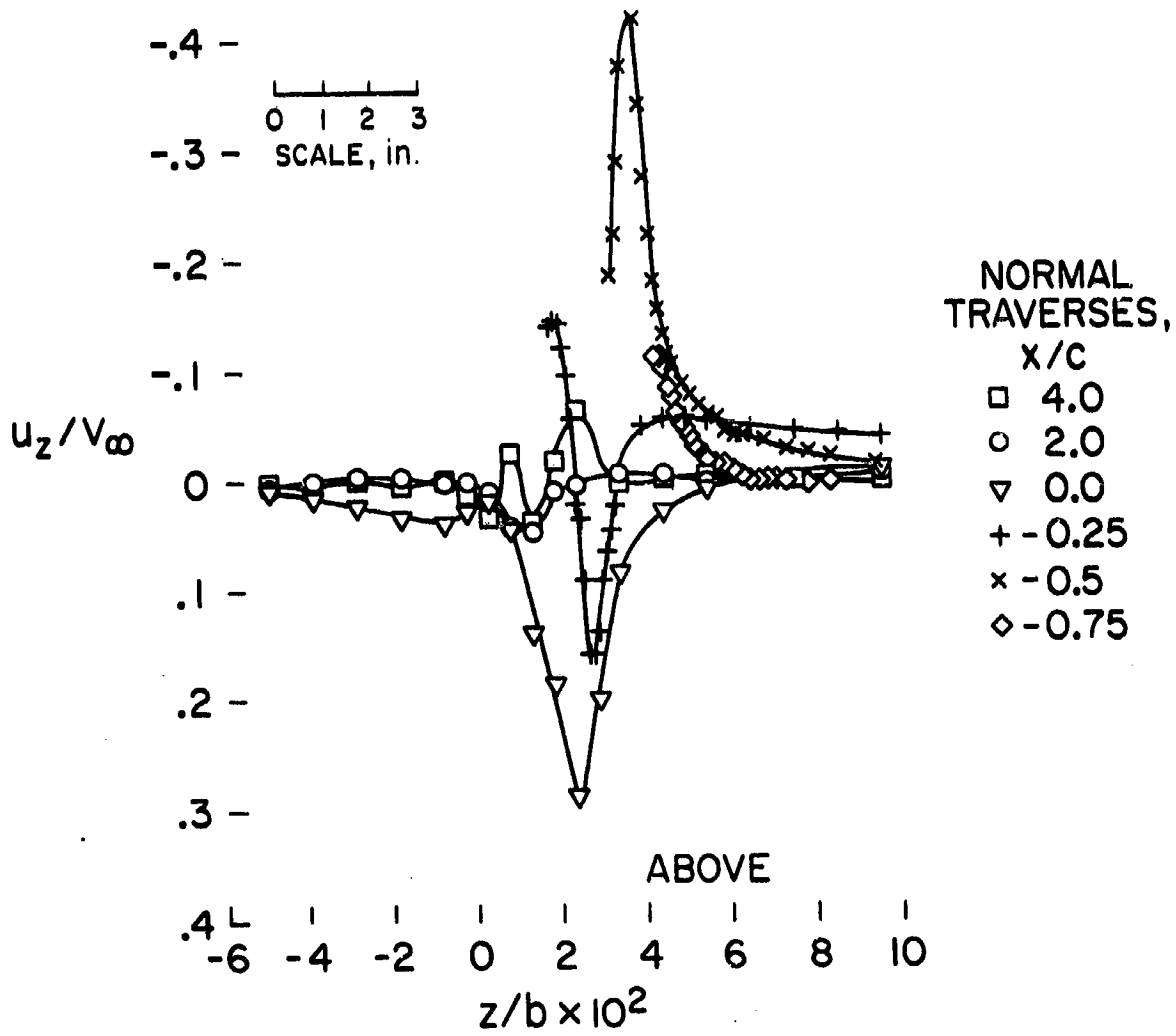


Figure 8.- Normal distribution of normal velocity.

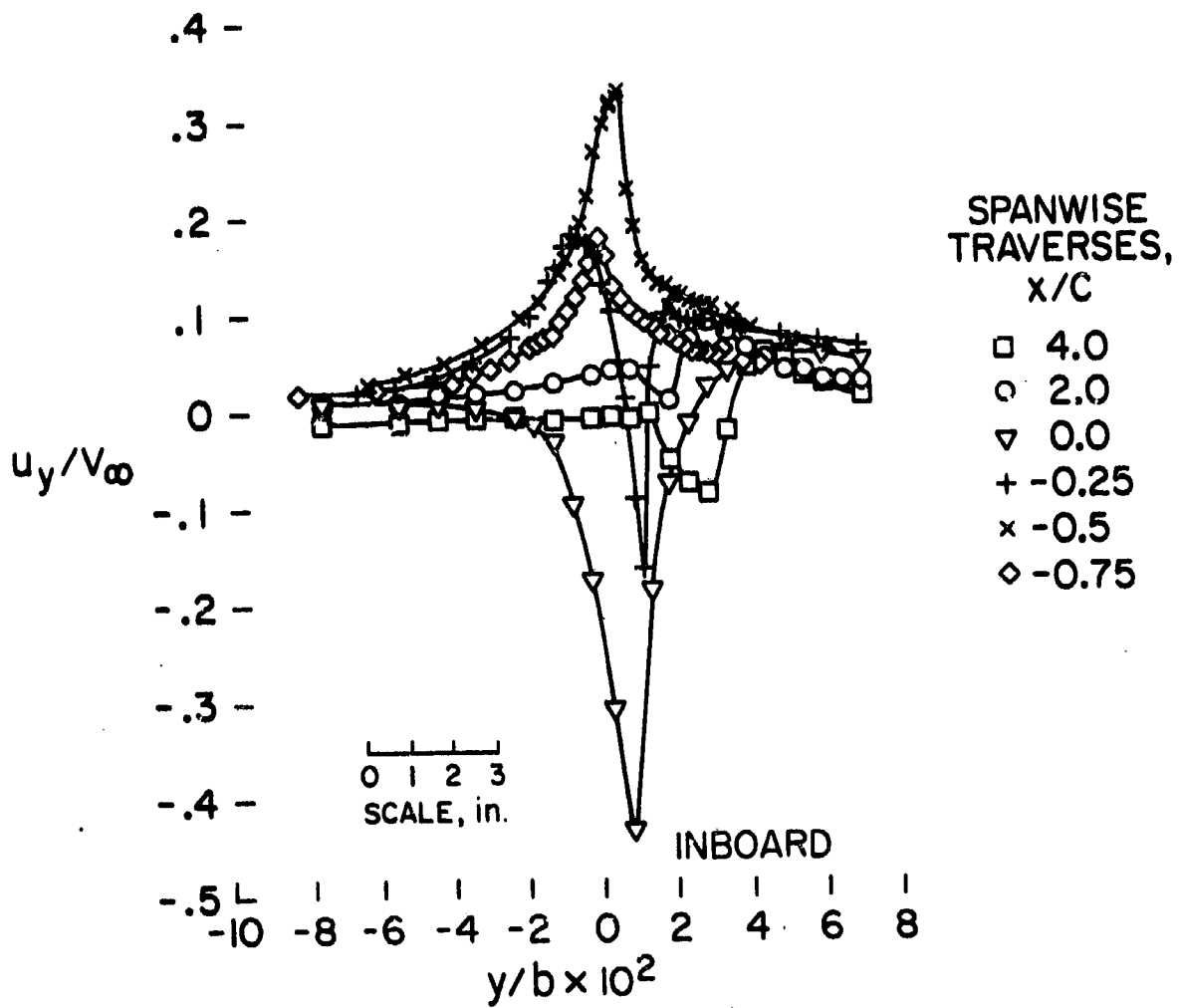


Figure 9.— Spanwise distribution of spanwise velocity.

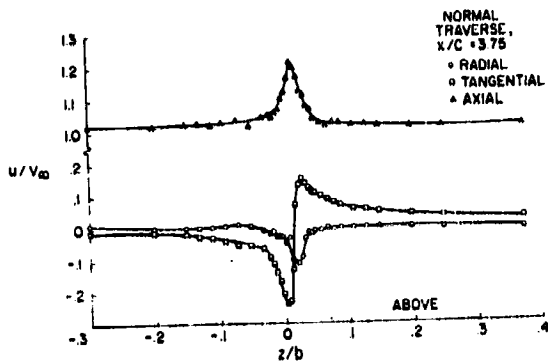


Figure 10.— Normal distribution of axial, circumferential, and radial velocity components $x/c = 3.75$.

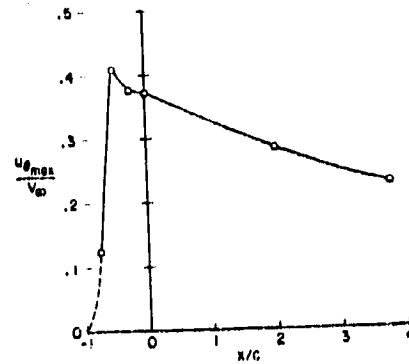


Figure 11.— Circumferential velocity maxima as function of streamwise distance.

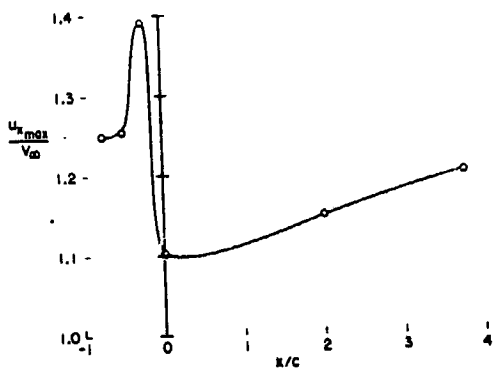


Figure 12.— Axial velocity maxima as function of streamwise distance.

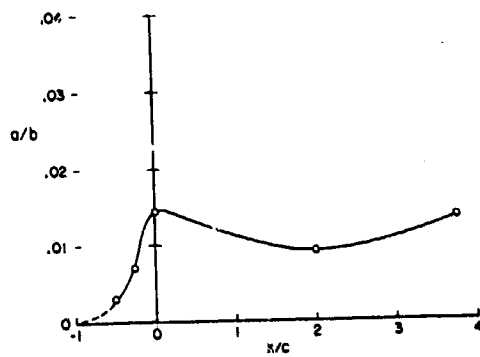


Figure 13.— Vortex core radius as function of downstream distance.

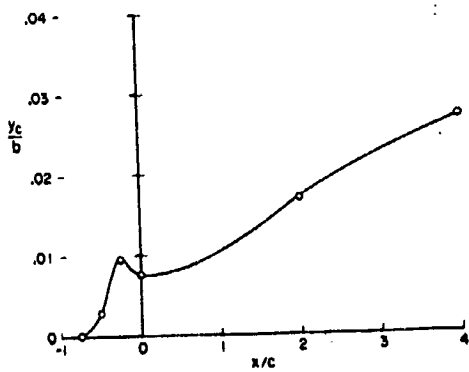


Figure 14.— Spanwise displacement of vortex centerline.

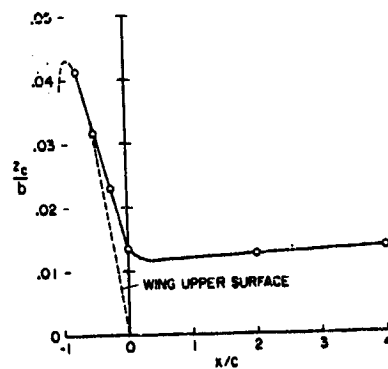


Figure 15.— Normal displacement of vortex